Materials Research Proceedings 28 (2023) 515-522 https://doi.org/10.21741/9781644902479-56

Friction extrusion processing of aluminum powders: Microstructure homogeneity and mechanical properties

CHAN Chang Yin-Cheng[1,a *], RATH Lars[1,b], SUHUDDIN Uceu F. H.[1,c] and KLUSEMANN Benjamin[1,2,d]

[1]Helmholtz-Zentrum Hereon, Institute of Materials Mechanics, Solid State Materials Processing, Max-Planck-Straße 1, 21502 Geesthacht, Germany

[2]Leuphana University Lüneburg, Institute for Production Technology and Systems, Universitätsallee 1, 21335 Lüneburg, Germany

[a]chang.chan@hereon.de, [b]lars.rath@hereon.de, [c]uceu.suhuddin@hereon.de, [d]benjamin.klusemann@hereon.de

Keywords: Friction Extrusion, Solid-State Processing, Aluminum, Powder Consolidation

Abstract. Friction extrusion (FE) is a solid-state process categorized as an energy-efficient process, utilizing the intrinsic friction-induced heat to plasticize and manufacture fully consolidated extrudate from various feedstocks, i.e. solid billet, chips and powder. Friction in the relative motion between the feedstock and the non-consumable die generates heat as well as imposes severe plastic deformation; this combination enables dynamic recrystallization and refinement of the microstructure. This study demonstrates the feasibility of directly extruding aluminum alloy powder into fully consolidated wire in a single step process. The extrudate is free of noticeable defects and shows predominantly homogeneous microstructure along the cross-section of the wire. The powder evolution upon passing through the die orifice was investigated in terms of morphology and microstructure. Additionally, the mechanical properties of the extrudate, i.e. microhardness and ultimate tensile strength, were compared to solid billets of AA7075 in different temper states and shows adequate mechanical properties without possible post-heat treatments.

Introduction

Friction extrusion (FE) process, developed and patented by Thomas et al. [1] in 1993, is used to extrude diverse materials, i.e. aluminum [2], magnesium [3] and copper [4] alloys. FE, schematically shown in Fig. 1, differs primarily from classical extrusion in the relative rotational motion, utilizing the well-established concept from friction stir welding (FSW). Friction occurs at the interface of the feedstock and the die, which introduces shear deformation and elevated temperature, resulting in the initiation of recrystallization and grain refinement. Three essential control factors in FE, i.e. axial force, rotational speed and die geometry, determine the extrudate properties and geometry, which have been extensively studied in the literature for different materials. The effect of the rotational speed and extrusion force was investigated and the rotational speed as the critical process parameter determined [5,6]. The die geometry not only defines extrudate shape but also affects the material flow prior to extrusion. Darshell et al. [7] and Halak et al. [8] discussed the influence of different die profiles and angles, respectively.

The FE from powder feedstock has attracted particular interest in the past few years, as it demonstrates the ability to extrude rod and tube directly from powder precursor [9,10] and led to better mechanical properties, such as ductility and electrical conductivity, compared to conventional analogous processing techniques [11]. Additionally, friction consolidation (FC) process that can be viewed as the FE without a die orifice, revealed the formation of the supersaturated solid solution of the immiscible alloy, which initiates the potential to achieve novel properties [12]. Strain and strain rate prior to FE are the decisive factors of the extrudate properties and have been studied using marker materials in solid billet feedstock [13]. In contrast to a solid billet feedstock, additional consolidation is necessary for powder FE. Furthermore, the influence of powder flow ability on strain and strain rate needs to be considered. Despite the numerous advantages of using powder as feedstock in FE and the possibility of accomplishing novel properties, the material flow of powder in front of the die is still rarely studied.

To understand the consolidation and deformation of the powder feedstock during FE, the present study analyzes the powder evolution within the residual feedstock, in particular of the powder shape alteration and the elimination of powder boundaries. In addition, the microstructure and properties of the extrudate are studied.

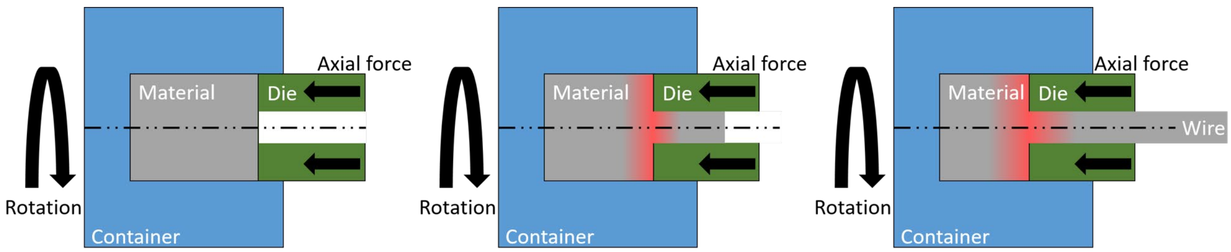

Fig. 1. Illustration of the FE process, including two machine parts, container and die.

Materials and Methods

Aluminum gas-atomized 7075 powder with a particle size smaller than 106 µm, stored in dry air, was used in this study. The dedicated friction extrusion machine FE100 manufactured by Bond Technologies was used. The machine allows forces up to 1000 kN, torques of 3500 Nm and rotational speeds of 1000 rpm. Along with high-speed data acquisition, FE100 enables the exploration of broad parameter combinations. The two essential tooling parts, shown in Fig. 1, namely a rotating powder container machined from 4140 steel with an inner diameter of 50 mm and a hydraulically driven extrusion die with a flat face from H13 steel with a 10 mm die orifice, were applied in the current study, which resulted in an extrusion ratio of 25. The temperature was recorded via type-K thermocouple embedded 1 mm from the extrusion die surface at a radius of 16.5 mm. The powders of ~ 150 g were filled in the powder container with a 0.6 mm AA7075 plate placed on top and pre-compacted with 100 kN to prevent powder spill before extrusion. The initial stage of the process applied a rotational speed of 300 rpm with 55 kN to establish complete contact between the extrusion die and the material. After the extrusion die advanced for 1 mm, the transition to the force-controlled friction extrusion process was conducted via a 10 s ramp. The constant 100 kN force with the powder container constantly rotating at 200 rpm were denoted as the process parameter in this study.

After extrusion, the extruded wire and the residual feedstock were sectioned transversely and longitudinally to the extrusion direction, respectively, and prepared following standardized metallography procedures. The microstructure of the wires was subjected to an additional electrolytic etching with Barker's solution at 20 V for 80 s and inspected with a Leica DMi8 optical microscope. In contrast, the microstructure of residual feedstock was analyzed by an FEI Quanta 650 field-emission scanning electron microscope (SEM) equipped with EDAX Apollo X energy dispersive X-ray spectroscopy (EDX). Furthermore, microhardness was tested with an EMCO-TEST Durascan 70 G5 with a load of 0.2 kg and ultimate tensile strength (UTS) was measured by an Imprintec i3D BVR according to DIN SPEC 4864. The mechanical properties of the extruded wire were compared with the as-received AA7075-T651 bar material and the annealed sample by heat treating the sample at 404 °C for 150 minutes followed by oven cooling.

Results and Discussion

The microstructure overview in the cross-section of the extrudate, processed at 100 kN and 200 rpm, is shown in Fig. 2. No noticeable defects and a fine-grained microstructure were observed in the core of the wire, indicating the powder is fully consolidated after FE. Grains, with grain size smaller than 10 µm, are predominantly present through the full cross-section of the wire, while at the periphery, larger grains up to 50 µm and defects can be noticed. The reasons might refer to the extensive residual heat in the die bearing promoting grain growth and the relative rotating motion between the extrudate and the die.

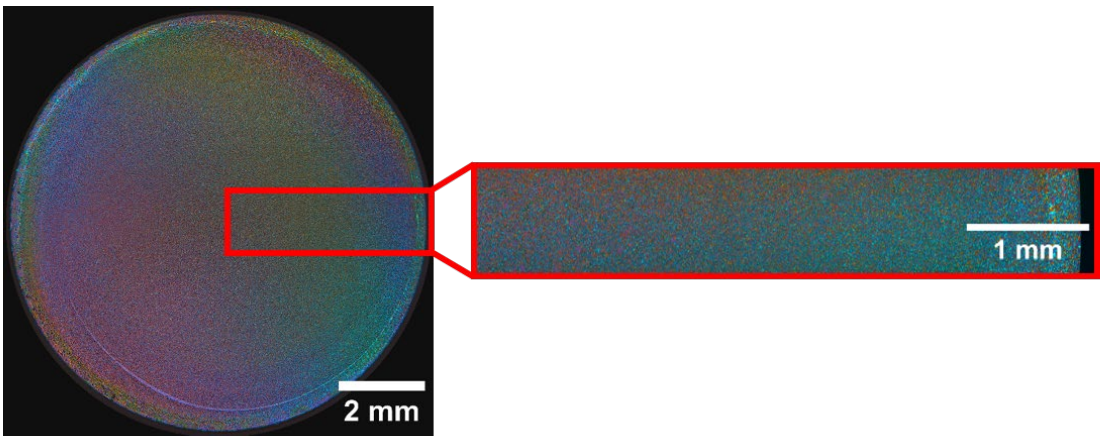

Fig. 2. Micrograph of etched cross-section of the wire extruded at 100 kN, 200 rpm, including enlarged section at the position highlighted by the red frame.

The powder evolution analysis is conducted on the residual feedstock after FE. The overview geometry of the specimen can be seen in Fig. 3(a). The left up and down corners of the specimen were fractured. Spherical raw powders, Fig. 3(b), have been found within the fracture area, indicating that the pre-compaction stage has not affected the powder in these regions prior to FE. Several positions at the center of the residual feedstock have been subjected to SEM for a powder evolution study. Fig. 3(c-g) reveals the evolution of powder during the FE process. High porosity has been identified as highlighted by white circles in Fig. 3(c) in form of void volume between as well as pores within individual powders, which is regarded as the starting condition of the powder after pre-compaction. The morphology of the powder alters gradually by approaching the die orifice and accompanies by the pores removal due to the extrusion force combined with the rising temperature and completed in Fig. 3(d). In Fig. 3(e), approximately 6 mm advanced entering the die orifice, the powders have been elongated in the extrusion direction, indicating the mechanical effect of the tooling has contributed to the FE. The powder boundaries begin to fade, suggesting the merge of the powder is potentially under the diffusion route with a much lower temperature, maximum 503 °C according to temperature measurement, compared to the conventional sintering temperature (580 – 620 °C) for AA7xxx alloys [14]. In Fig. 3(f), the large amount of powder boundaries vanishes and suggests that the powder consolidation nearly finished prior to entering the die orifice and material flow onwards can be considered similar to FE from a solid billet feedstock. However, the different strengths and the flow ability among the pre-compacted powder, solid billet or chips have a tremendous impact on the initial heat generation and the heat dissipation,

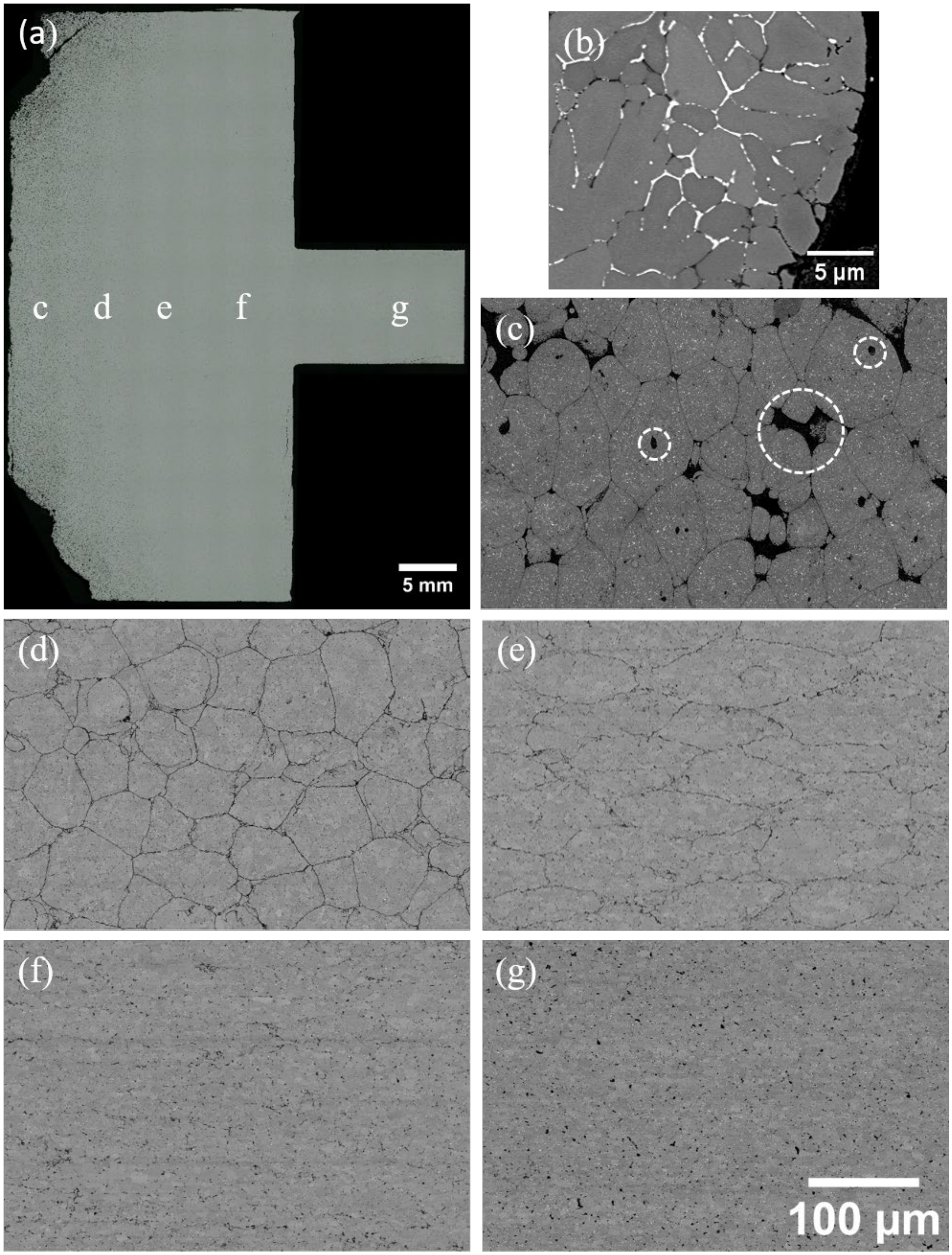

Fig. 3. Overview of residual feedstock (a), base powder (b) and powder evolution in the center from the left of the specimen (c) to the extrudate (g).

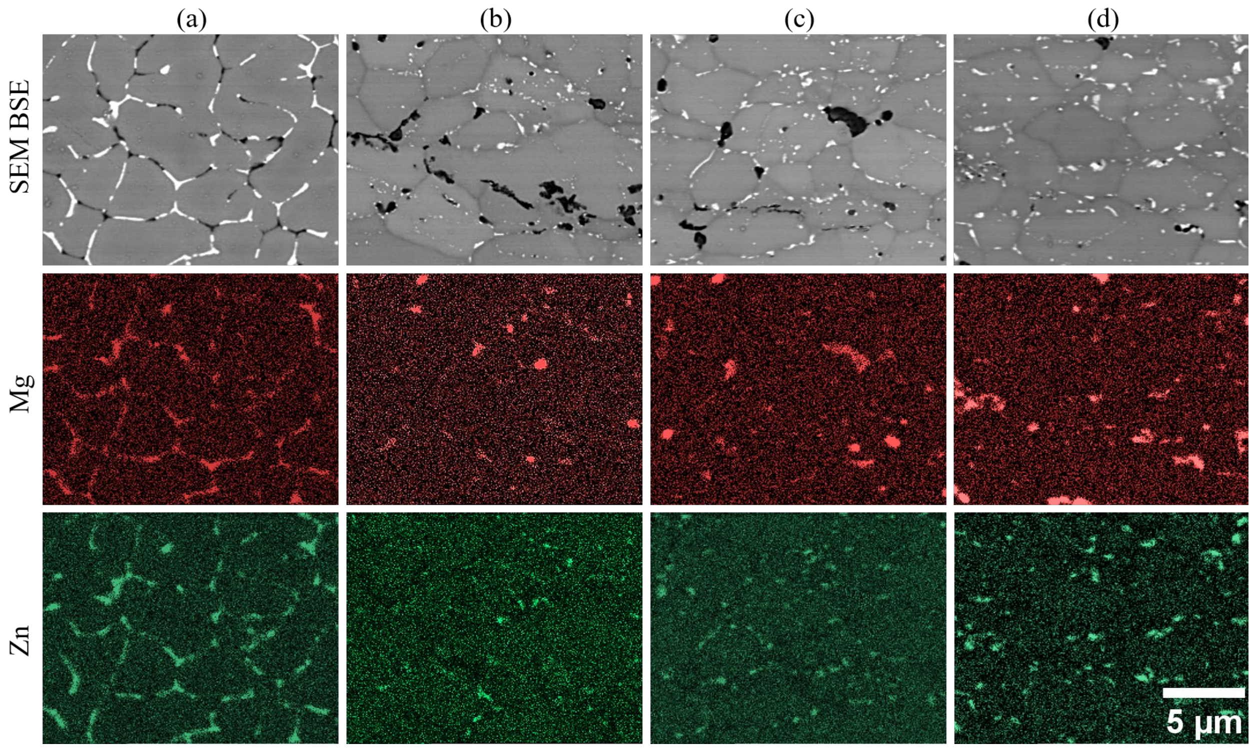

Fig. 4. SEM backscatter images from base powder (a) and different distance to the die orifice, i.e. 6 mm (b) and 4 mm (c) advanced and 10 mm (d) retreated, and the corresponding EDX mapping of Mg and Zn.

which hinder the direct implantation of the strain and strain rate found in the literature for solid billet as well as chips feedstock into the powder [13, 15]. After passing through the die orifice, the microstructure of the extrudate transforms into the final microstructure as shown at the position of 10 mm, Fig. 3(g), after the die orifice. No powder boundary has been found, indicating the powder is fully consolidated after the FE and further confirming the previous finding in Fig. 2.

In the aluminum alloy AA7075, two major alloying elements, magnesium and zinc, form the $MgZn_2$ phase at the grain boundary, which is observed in all the SEM images as white particles. Therefore, the residual feedstock is subjected to EDX to disclose and complement the powder evolution in the FE before entering the extrusion orifice. The EDX mapping of the Mg and Zn as well as the corresponding SEM backscatter images are shown in Fig. 4(a-d). In the base powder, Fig. 4(a), most of the $MgZn_2$ phases are larger and located at the grain boundary, which is the typical behavior of this phase in AA7075. The discontinuity observed in the EDX mapping can be explained by the re-melting of solid particles [16]. Approaching the extrusion die, the $MgZn_2$ phases are fragmented into smaller particles under shear and longitudinal deformation or diffuse into the grains as reported that FE can form a forced supersaturated solid solution [12]. By comparing the different grain orientations in the raw powder, Fig. 3(b), and near the extrusion die, Fig. 4(b-d), the transformation of the randomly distributed grains aligned in the extrusion direction can be observed, indicating the effect of the deformation. In Fig. 4(b), the capture position is adjacent to the powder boundary, where the $MgZn_2$ phases are rarely found, which corresponds to the observation of the unprocessed base powder. The reason could be that the rapid solidification rate of gas-atomized powder impedes the diffusion behavior of alloying elements on the powder surface [16]. Since the melting point of $MgZn_2$ phases is much below the processing temperature of FE, the incipient melting of existing phases may occur before the die orifice and could explain the smaller defects observed in Fig. 4(c). However, the huge defects may be due to the isolated pores that typically find in powder metallurgy materials [17]. It needs to be mentioned that the grain size observed in the SEM images is also below 10 µm and comparable to the base powder.

The microhardness was evaluated over the cross-section for a part in the middle of the extrudate, see Fig. 5(a). The FE extrudate shows a relatively homogeneous hardness, 115.6 HV, except for the outer ring with slightly larger grains. At the lower part of the mapping, one region with significantly lower microhardness is supposed to be a defect, as observed at the periphery of the cross-section in Fig. 2. By comparing the extrudate to AA7075 alloys in different temper states, T6 and O, Fig. 5(b), the hardness is 67 % of AA7075-T6 and 80 % higher than the annealed state. AA7075 is a precipitate hardenable alloy, and T6 temper is the peak artificial aging. Therefore, the lower hardness after high temperature exposure during FE (maximum measured temperature of 503 °C) is expected due to the dissolution of strengthening precipitates.

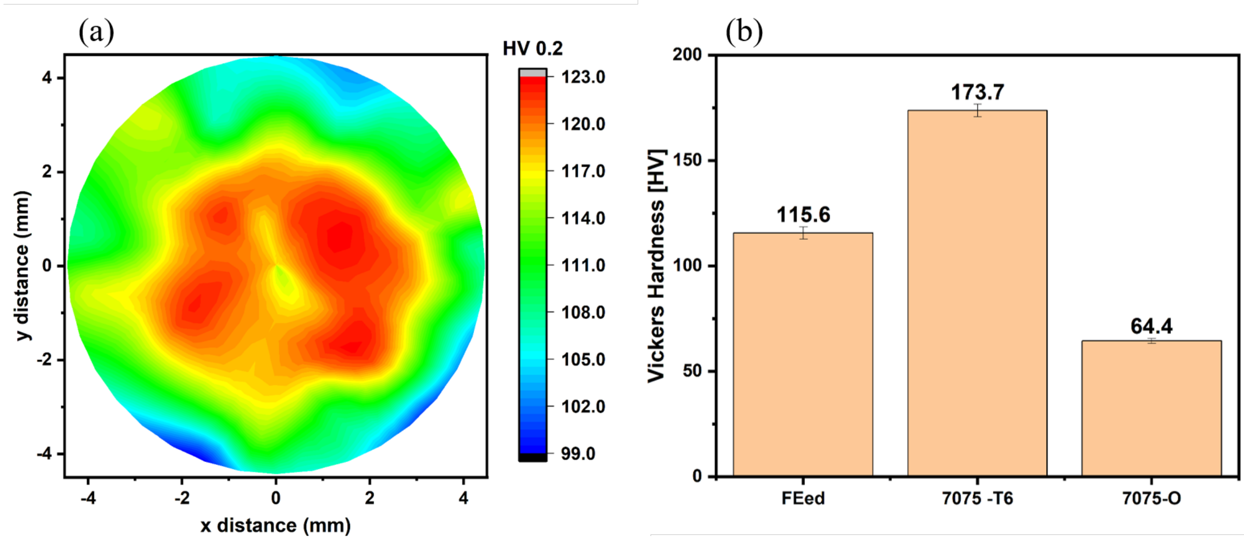

Fig. 5. Microhardness mapping of the cross-section for the extrudate (a) and comparison to the base material in different temper states.

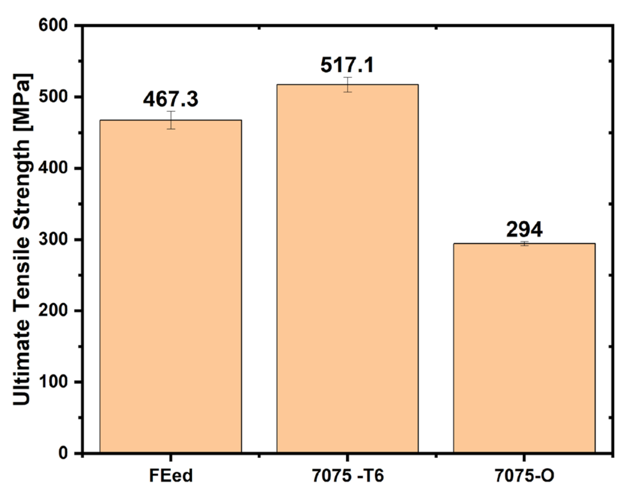

Fig. 6. Ultimate tensile strength for the extrudate and comparison to the base material in different temper states.

The UTS of the FE extrudate as well as for AA7075-T6 and AA7075-O is shown in Fig. 6. The extrudate UTS is 467.3 MPa, which shares the same trend as the microhardness, with 90 % of the T6 state and 59 % more than the annealed state. The recrystallization and the grain refinement enabled the improvement of the mechanical properties; however, the precipitate strengthening effect dictated the mechanical properties of 7075 alloys, and the further increase of UTS after artificial aging has been proven [18]. The UTS value is comparable to the FE from AA7075 solid billet feedstock [8, 18], indicating full consolidation of the powder during FE.

Summary

In the present study, friction extrusion based on powder material was investigated in terms of extrudate microstructure as well as powder evolution in front of the extrusion orifice. The fully consolidated wire was successfully extruded directly from the powder feedstock. Additionally, the mechanical properties of the final extrudate were analyzed. The main findings are summarized as follows:

- Fully consolidated wire with predominantly homogeneously distributed fine grains and no noticeable defects in the core is successfully extruded from powder feedstock without a complex powder metallurgy procedure. Larger grains and defects are observed at the periphery of the wire; hence, a cooling system has been planned to introduce to prevent the grain coarsening issue.
- The combination of pressure and elevated temperature leads to extensive porosity removal within the powder feedstock, followed by the elongation of powder particles in the extrusion direction as well as the elimination of powder boundaries finally forming the consolidated extrudate.
- Adequate mechanical properties without post-heat treatment, comparable results to extrusion from solid billet feedstock, and the potential to improve the properties by applying artificial aging are achieved and demonstrated.

Funding

This project has received funding from the European Research Council (ERC) under the European Union’s Horizon 2020 research and innovation programme (grant agreement No 101001567).

Data Availability

The data related to this research will be made available online.

References

[1] W.M. Thomas, E.D. Nicholas and S.B. Jones, U.S. Patent 5,262,123. (1993).
[2] W. Tang, A.P. Reynolds, Production of wire via friction extrusion of aluminum alloy machining chips, J. Mater. Process. Technol. 210 (2010) 2231-2237. https://doi.org/10.1016/j.jmatprotec.2010.08.010
[3] G. Buffa, D. Campanella, L. Fratini, F. Micari, AZ31 magnesium alloy recycling through friction stir extrusion process, Int. J. Mater. Form. 9 (2016) 613-618. https://doi.org/10.1007/s12289-015-1247-6
[4] X. Li, N. Overman, T. Roosendaal, M. Olszta, C. Zhou, H. Wnag, T. Perry, J. Schroth, G. Grant, Microstructure and Mechanical Properties of Pure Copper Wire Produced by Shear Assisted Processing and Extrusion, JOM 71 (2019) 4799-4805. https://doi.org/10.1007/s11837-019-03752-w
[5] M.A. Ansari, R.A. Behnagh, M. Narvan, E.S. Naeini, M.K.B. Givi, H. Ding, Optimization of Friction Stir Extrusion (FSE) Parameters Through Taguchi Technique, Trans. Indian Inst. Met. 69 (2016) 1351-1357.

[6] D. Baffari, A.P.Reynolds, X. Li, L. Fratini, Influence of processing parameters and initial temper on Friction Stir Extrusion of 2050 aluminum alloy, J. Manuf. Process. 28 (2017) 319-325. https://doi.org/10.1016/j.jmapro.2017.06.013
[7] J.T. Darsell, N.R. Overman, V.V. Joshi, S.A. Whalen, S.N. Mathaudhu, Shear Assisted Processing and Extrusion (ShAPE™) of AZ91E Flake: A Study of Tooling Features and Processing Effects, J. Mater. Eng. Perform. 27 (2018) 4150-4161. https://doi.org/10.1007/s11665-018-3509-1
[8] R.M. Halak, L. Rath, U.F.H.R. Suhuddin, J.F. dos Santos, B. Klusemann, Changes in processing characteristics and microstructural evolution during friction extrusion of aluminum, Int. J. Mater. Form. 15 (2022) 24. https://doi.org/10.1007/s12289-022-01670-y
[9] S. Whalen, M. Olszta, C. Roach, J. Darsell, D. Graff, M. Reza-E-Rabby, T. Roosendaal, W. Daye, T. Pelletiers, S. Mathaudhu, N. Overman, High ductility aluminum alloy made from powder by friction extrusion, Materialia 6 (2019) 100260. https://doi.org/10.1016/j.mtla.2019.100260
[10] X. Li, T. Wang, X. Ma, N. Overman, S. Whalen, D. Herling, K. Kappagantula, Manufacture aluminum alloy tube from powder with a single-step extrusion via ShAPE, J. Manuf. Process. 80 (2022) 108-115. https://doi.org/10.1016/j.jmapro.2022.05.060
[11] X. Li, C. Zhou, N. Overman, X. Ma, N. Canfield, K. Kappagantula, J. Schroth, G. Grant, Copper carbon composite wire with a uniform carbon dispersion made by friction extrusion, J. Manuf. Process. 65 (2021) 397-406. https://doi.org/10.1016/j.jmapro.2021.03.055
[12] M. Komarasamy, X. Li, S.A. Whalen, X. Ma, N. Canfield, M.J. Olszta, T. Varga, A.L. Schemer-Kohrn, A. Yu, N.R. Overman, S.N. Mathaudhu, G.J. Grant, Microstructural evolution in Cu–Nb processed via friction consolidation, J. Mater. Sci. 56 (2021) 12864-12880. https://doi.org/10.1007/s10853-021-06093-9
[13] X. Li, M. Reza-E-Rabby, A. Guzman, G. Grant, S. Mathaudhu, M. Hinton, A. Reynolds, Strain and strain rate in friction extrusion, J. Mater. Res. Technol. 22 (2022) 882-893. https://doi.org/10.1016/j.jmrt.2022.07.116
[14] G.B. Schaffer, S.H. Huo, On development of sintered 7xxx series aluminium alloys, Powder Metall. 42 (1999) 219-226. https://doi.org/10.1179/003258999665558
[15] D. Baffari, G. Buffa, D. Campanella, L. Fratini, A.P. Reynolds, Process mechanics in Friction Stir Extrusion of magnesium alloys chips through experiments and numerical simulation, J. Manuf. Process. 29 (2017) 41-49. https://doi.org/10.1016/j.jmapro.2017.07.010
[16] M.R. Rokni, C.A. Widener, G.A. Crawford, Microstructural evolution of 7075 Al gas atomized powder and high-pressure cold sprayed deposition, Surf. Coat. Technol. 251 (2014) 254-263. https://doi.org/10.1016/j.surfcoat.2014.04.035
[17] A. Hadrboletz, B. Weiss, Fatigue behaviour of iron based sintered material: a review, Int. Mater. Rev. 42 (1997) 1-44. https://doi.org/10.1179/imr.1997.42.1.1
[18] R. Kalsar, X. Ma, J. Darsell, D. Zhang, K. Kappagantula, D.R. Herling, V.V. Joshi, Microstructure evolution, enhanced aging kinetics, and mechanical properties of AA7075 alloy after friction extrusion, Mater. Sci. Eng. A. 823 (2022) 142575. https://doi.org/10.1016/j.msea.2021.142575